Magnonic band gaps in YIG-based one-dimensional magnonic crystals: An array of grooves versus an array of metallic stripes

V. D. Bessonov,[1,2] M. Mruczkiewicz,[3] R. Gieniusz,[1] U. Guzowska,[1] A. Maziewski,[1] A. I. Stognij,[4] and M. Krawczyk[3,*]

[1]*Faculty of Physics, University of Białystok, Białystok, Poland*

[2]*Institute of Metal Physics, Ural Division of Russian Academy of Sciences, Yekaterinburg, Russia*

[3]*Faculty of Physics, Adam Mickiewicz University in Poznan, Umultowska 85, Poznań, Poland*

[4]*Scientific-Practical Materials Research Center at National Academy of Sciences of Belarus, Minsk, Belarus*

(Received 9 December 2014; revised manuscript received 10 March 2015; published 23 March 2015)

We present an experimental and theoretical study of magnonic band gaps in planar one-dimensional magnonic crystals of two types, with a periodic array of metallic stripes or a periodic array of grooves on an yttrium iron garnet film. Propagating magnetostatic surface spin waves are excited in the considered periodic magnetic structures and measured by microstripe transducers with a vector network analyzer and with a Brillouin light scattering spectroscopy. The properties of magnonic band gaps are explained and illustrated by finite element method calculations. We demonstrate a major influence of the nonreciprocal spin-wave dispersion properties induced by metallic stripes on the width of the magnonic band gap and its dependence on the external magnetic field. The indirect character of the band gap and the higher group velocity of spin waves in the metallic magnonic crystal are identified as the main causes of the wider band gap and steeper decrease in its width with increasing magnetic field in this structure as compared to the grooved magnonic crystal. Potential applications of both types of magnonic crystals and prospects for their miniaturization are discussed as well.

DOI: 10.1103/PhysRevB.91.104421 PACS number(s): 75.75.−c, 76.50.+g, 75.30.Ds

I. INTRODUCTION

The spatial periodicity determines the rule of conservation of quasimomentum for excitations in artificial crystals, similar to the conservation of momentum in homogeneous materials. In the frequency domain this periodicity results in the formation of pass bands and band gaps, the latter being frequency ranges in which no excitation states are available and wave propagation is prohibited. The study of magnetic structures with artificial translational symmetry is aimed at the design of new materials, referred to as metamaterials, with properties unseen in nature and thus otherwise impossible. In particular, artificial ferromagnetic materials known as magnonic crystals (MCs), with a periodicity comparable to the wavelength of spin waves (SWs) [1–3], have recently aroused much interest from researchers in physics. A typical example of application of MCs is the control of the propagation and scattering of SWs. The first experimental study of magnetostatic SWs in a ferromagnetic thin film with a periodic surface was carried out by Sykes *et al.* as early as 1976 [4]. The number of studies on MCs has much increased since that time and continues to grow rapidly because of the interesting physics of these materials and their potential applications [5–8].

In this paper we present complementary experimental and theoretical investigations of SWs, studied versus the amplitude of the external magnetic field, in two types of MCs with the same periodicity. One MC has a periodic system of grooves etched in a yttrium iron garnet (YIG) film. The other is a uniform YIG crystal with an array of metallic stripes atop. Studies of structures of both types have already been reported [9–14]. Representing the first type, an SW waveguide was proposed and investigated experimentally as a delay line or filter for microwave applications [4,15,16], and more recently as a basic element of a purely magnonic transistor [17] or a microwave phase shifter [18]. Also considered as delay lines and filters [16,19], structures of the other type have recently been proposed as room-temperature magnetic field sensors as well [20–22].

We perform a comparative study of the magnonic band structure of these two types of MCs magnetically saturated by an external magnetic field applied along the grooves or metallic stripes. A passive delay line with a network analyzer and the space-resolved Brillouin light scattering (BLS) technique are used in the measurements. The SW dynamics is modeled by the finite element method (FEM) in the frequency domain. On the basis of the obtained calculation results we explain the experimental data and discuss the properties of the magnonic band gaps in these two types of MCs. We also investigate the dependence of the magnonic band gap on the amplitude of the applied magnetic field, and obtain numerical results in very good agreement with the experimental data. We show that the differences in that dependence between the two MCs result from the character of the magnonic band gaps, direct in the case of grooves and indirect in the structure with Au stripes. Analysis of the imaginary part of the wave vector within the band gap proves to be a useful approach for the explanation of the observed dependencies. Finally, we use the acquired information to discuss the suitability of the considered two types of MCs for recently proposed applications.

The paper is organized as follows. In Sec. II we briefly describe the experimental methods used in our study for the measurement of the SW transmission with microwave transducers and space-resolved BLS. In Sec. III we present the finite-element method used for the calculation of the magnonic band structure. In the following Sec. IV we discuss the results obtained for the two types of MCs. The closing Sec. V provides a summary of the paper.

*krawczyk@amu.edu.pl

II. EXPERIMENTS

The fabrication process of the artificial periodic structures with characteristic dimensions in deep nanoscale is very hard to control and so far mainly theoretical studies are available in this scale [23,24]. In particular, it concerns the quality of the edges and the interfaces between adjacent materials which make up MC and can significantly influence magnonic band structure [25–27]. However, in larger scale with a period starting from 100 nm the fabrication technology is already well established for thin ferromagnetic metallic films [28,29]. The YIG films of a thickness of tens of nanometers have been fabricated only recently and the quality of these films increases systematically. The damping comparable to the value in thick YIG films (of order smaller than in the best metallic ferromagnetic film) has already been achieved [30,31]. However, the YIG thin films with patterning in nanoscale is not yet investigated. Here, we study dielectric YIG films structurized in larger scale where edge properties have a minor influence on the SW dynamics. Thick YIG films (10 μm) were epitaxially grown on gallium gadolinium garnet (GGG) substrates in a (111) crystallographic plane and served to fabricate one-dimensional (1D) MCs. The MCs used in our experiment had been produced in the form of the waveguide of 3.5 mm in width and 50 mm in length with (i) an array of parallel grooves chemically etched [sample A, Fig. 1(a)] and (ii) an array of Au microstripes placed on the top of the film [sample B, Fig. 1(b)]. The grooves and Au microstripes were perpendicularly oriented with respect to the SW propagation direction and include nine lines of 80-μm width which are spaced 70 μm from each other, so that the period a is 150 μm.

The external magnetic field H_0 is applied along the grooves and microstripes in order to form conditions for propagation of the magnetostatic surface spin wave (MSSW), also called the Damon-Eshbach wave. This wave has asymmetric distribution of the SW amplitude across the film, which depends on the direction of the magnetic field with respect to the direction of the wave vector, and this asymmetry increases with increasing wave number. By putting metal on the ferromagnetic film the nonreciprocal dispersion relation of MSSW is induced [32].

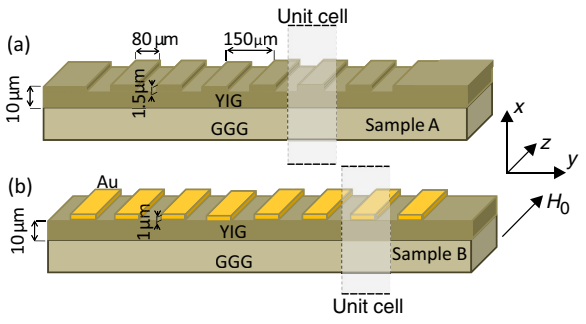

FIG. 1. (Color online) Geometry of the two MCs investigated in this paper. (a) Sample A, a 1D MC created by etching an array of grooves in a YIG film on a GGG substrate. The film is 10 μm thick, and the grooves are 80 μm wide and 1.5 μm deep. (b) Sample B, a 1D MC obtained by the deposition of an array of Au stripes on a 10-μm-thick homogeneous YIG film. The stripes are 80 μm wide and 1 μm thick. Both samples have the same lattice constant of 150 μm.

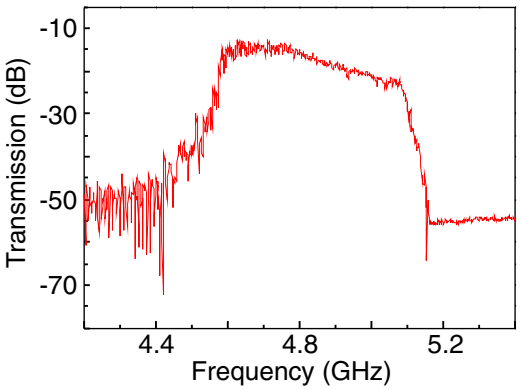

FIG. 2. (Color online) Transmission spectra of MSSW in the reference sample, i.e., uniform YIG film of 10 μm thickness in the external magnetic field 0.1 T.

The MSSWs were excited and detected in the garnet film waveguide using two 30-μm wide microstripe transducers connected with the microwave vector network analyzer (VNA), one placed in front and another one behind the periodic structure. An external magnetic field ($\mu_0 H_0 = 0.1$ T) was strong enough to saturate the samples. Microwave power of 1 mW used for the input transducer was sufficiently small in order to avoid any nonlinear effects. A VNA was used to measure transmission spectra collected for the second transducer. The transmission spectra of SWs measured in the reference sample, i.e., a thin YIG film, is shown in Fig. 2. The transmission of the microwave signal above 10 dB is in the band from 4.46 to 5.14 GHz.

In BLS measurements the SWs were excited with the single 30-μm-wide microwave transducer located in front of the array of Au microstripes (sample B). The SWs scattered on the line of the waveguide were detected by space-resolved BLS spectroscopy in the forward scattering configuration [33]. The probe laser beam was scanned across the sample (in the areas between Au stripes) and the BLS intensity, which is proportional to the square of the dynamic magnetization amplitude, was recorded at various points. This technique allows for a two-dimensional (2D) mapping of the spatial distribution of the SW amplitude with step sizes of 0.02 mm.

III. THEORETICAL MODELING

In our calculations we assume the stripes and grooves have infinite length (i.e., they are infinite along the z axis). This is a reasonable assumption taking into account that the length is around 23 times longer than the period of the structure. The structures under investigation remain in a magnetically saturated state along the z axis due to the static external magnetic field pointing in the same direction.

To obtain insight into the formation of the magnonic band structure and opening magnonic band gaps the numerical calculations of the dispersion relation were performed. For SWs from the GHz frequency range, due to the 10-μm thickness of the YIG film and a small value of the exchange constant in YIG, the exchange interactions can be safely neglected. In order to calculate the SW dispersion relation in magnetostatic approximation we solved the wave equation

for the electric field vector **E** [34]:

$$\nabla \times \left(\frac{1}{\hat{\mu}_r(\mathbf{r})} \nabla \times \mathbf{E} \right) - \omega^2 \sqrt{\epsilon_0 \mu_0} \left(\epsilon_0 - \frac{i\sigma}{\omega \epsilon_0} \right) \mathbf{E} = 0, \quad (1)$$

where $\omega = 2\pi f$, f is an SW frequency, μ_0 and ϵ_0 denote the vacuum permeability and permittivity, respectively, and σ is conductivity, different from zero only in sample B. To describe the dynamics of the magnetization components in the plane perpendicular to the external magnetic field, it is sufficient to solve Eq. (1) for the z component of the electric field vector **E** which depends solely on the x and y coordinates, $E_z(x,y)$ [35].

The permeability tensor $\hat{\mu}(\mathbf{r})$ in Eq. (1) can be obtained from the Landau-Lifshitz (LL) equation [32]. The assumption that the magnetization is in the equilibrium configuration allows us to use the linear approximation in SW calculations, which implies small deviations of the magnetization vector $\mathbf{M}(\mathbf{r},t)$ from its equilibrium orientation. Thus, for the MCs saturated along the z axis, the magnetization vector can split into the static and dynamic parts: $\mathbf{M}(\mathbf{r},t) = M_z\hat{z} + \mathbf{m}(\mathbf{r},t)$, and we can neglect all nonlinear terms with respect to dynamical components of the magnetization vector $\mathbf{m}(\mathbf{r},t)$ in the equation of motion defined below. Since $|\mathbf{m}(\mathbf{r},t)| \ll M_z$, we can assume also $M_z \approx M_S$, where M_S is the saturation magnetization. We consider only monochromatic SWs propagating along the direction of the periodicity, thus we can write $\mathbf{m}(\mathbf{r},t) = \mathbf{m}(x,y)\exp(i\omega t)$. Under these assumptions the dynamic of the magnetization vector $\mathbf{m}(\mathbf{r})$ with negligible damping is described by the stationary LL equation:

$$i\omega \mathbf{m}(\mathbf{r}) = \gamma \mu_0 \left[M_S \hat{z} + \mathbf{m}(\mathbf{r}) \right] \times \mathbf{H}_{\text{eff}}(\mathbf{r}), \quad (2)$$

where γ is the gyromagnetic ratio (we assume $\gamma = 176$ rad GHz/**T**) and $\mathbf{H}_{\text{eff}}$ denotes the effective magnetic field acting on the magnetization. The effective magnetic field is in general a sum of several components; here we will consider two terms, the static external magnetic field and the dynamic magnetostatic field:

$$\mathbf{H}_{\text{eff}}(\mathbf{r},t) = H_0\hat{z} + \mathbf{h}_{\text{ms}}(\mathbf{r},t). \quad (3)$$

The permeability tensor $\hat{\mu}(\mathbf{r})$ in Eq. (1) obtained from the linearized damping-free LL Eq. (2) for ferromagnetic material takes the following form:

$$\hat{\mu}_r = \begin{pmatrix} \mu^{xx} & i\mu^{xy} & 0 \\ -i\mu^{yx} & \mu^{yy} & 0 \\ 0 & 0 & 1 \end{pmatrix}, \quad (4)$$

where

$$\mu^{xx} = \frac{\gamma\mu_0 H_0(\gamma\mu_0 H_0 + \gamma\mu_0 M_S) - \omega^2}{(\gamma\mu_0 H_0)^2 - \omega^2}, \quad (5)$$

$$\mu^{xy} = \frac{\gamma\mu_0 M_S \omega}{(\gamma\mu_0 H_0)^2 - \omega^2}, \quad (6)$$

$$\mu^{yx} = \mu^{xy}, \quad \mu^{yy} = \mu^{xx}; \quad (7)$$

in nonmagnetic areas permeability is an identity matrix.

Equation (1) with the permeability tensor defined in Eq. (4) in the periodic structure has solutions which shall fulfill the Bloch theorem:

$$E_z(x,y) = E'_z(x,y)e^{ik_y y}, \quad (8)$$

where $E'_z(x,y)$ is a periodic function of y: $E'_z(x,y) = E'_z(x,y+a)$. k_y is a wave vector component along y and a is a lattice constant. Due to considering SW propagation along the y direction only, we assume $k_y \equiv k$. Equation (1) together with Eq. (8) can be written in the weak form and the eigenvalue problem can be generated, with the eigenvalues being frequencies of SWs or in the inverse eigenproblem with the wave numbers as eigenvalues. The former eigenproblem is used to obtain the magnonic band structure, the latter to calculate the complex wave number of SW inside the magnonic band gaps. This eigenequation is supplemented with the Dirichlet boundary conditions at the borders of the computational area placed far from the ferromagnetic film along the x axis (bold dashed lines in Fig. 1).

In FEM the equations are solved on a discrete mesh in the two-dimensional real space [in the plane (x, y)] limited due to the Bloch equation to the single unit cell (marked by the gray box in Fig. 1). In this paper we use one of the realizations of FEM developed in the commercial software COMSOL MULTIPHYSICS Version 4.2. This method has already been used in calculations of magnonic band structure in thin 1D MCs, and their results have been validated by comparing with micromagnetic simulations and experimental data [36–38]. The detailed description of FEM in its application to calculation of the SW spectra in MCs can be found in Refs. [38,39].

In calculations we have taken nominal values of the MC dimensions and the saturation magnetization of YIG as $M_S = 0.14 \times 10^6$ A/m. The conductivity of the metal is assumed as $\sigma = 6 \times 10^7$ S/m, which is a tabular value for Au.

IV. RESULTS AND DISCUSSION

In Figs. 3(a) and 3(b) we present the results of the SW transmission measurements with the use of microstripe lines in the external magnetic field 0.1 T for sample A and sample B, respectively. We can see a clear evidence of three (centered at 4.81, 4.97, and 5.05 GHz) and two magnonic band gaps

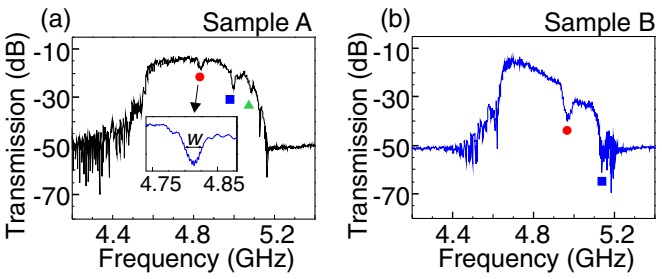

FIG. 3. (Color online) Transmission spectra of SWs in (a) sample A and (b) sample B measured with microstripe lines in external magnetic field 0.1 T. The magnonic band gaps are marked by solid symbols: In sample A there are three gaps, and in sample B there are two gaps, however, the second gap is at the part of low transmission and will not be considered in the paper. In the inset of (a) the enlargement of the spectra around the first band gap is shown; the width of this gap is w.

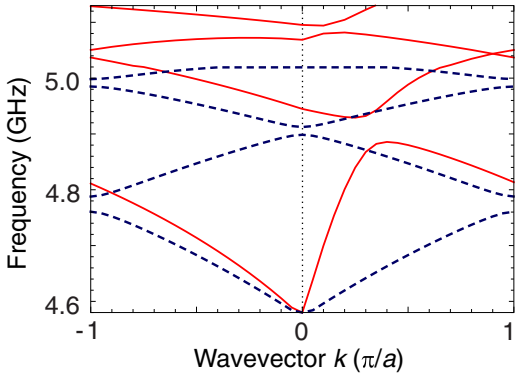

FIG. 4. (Color online) Magnonic band structure in the first Brillouin zone calculated for sample A (blue dashed line) and sample B (red solid line) with magnetic field $\mu_0 H_0 = 0.1$ T. Magnonic band structure is symmetric and asymmetric with respect to the Brillouin zone center (marked by the vertical black dashed line) in samples A and B, respectively.

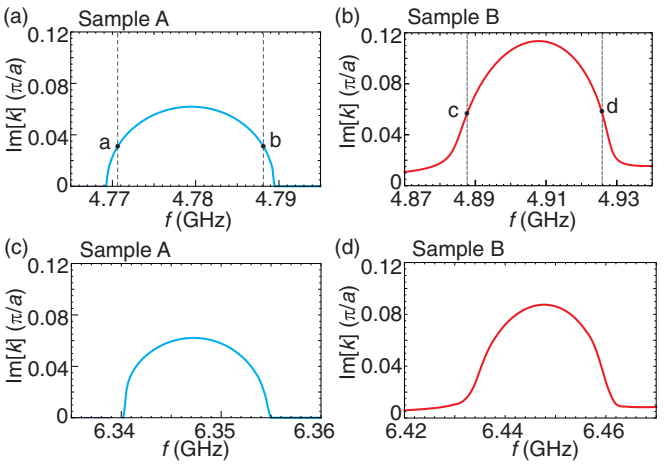

FIG. 5. (Color online) The imaginary part of the wave number around the first band gap in sample A (a) and (c), and in sample B (b) and (d), for the two values of the magnetic field $\mu_0 H_0 = 0.1$ T (a) and (b) and 0.15 T (c) and (d). The calculations were done for the inverse eigenproblem with FEM. The letters a–d indicate points where the value of Im[k] takes one-half of its maximum. These points may indicate the borders of the band gap extracted from the transmission measurements.

(at 4.88 and 5.05 GHz) in sample A and B, respectively. The transmission band in both samples is approximately the same as in the reference sample (Fig. 2), however, at high frequencies in sample B a large decrease of the transmission magnitude is observed. Thus, in MC with metallic stripes the second magnonic band gap [marked with a blue square in Fig. 3(b)] is already at the part of the low transmission. The estimation of its position and width will be loaded with additional errors and some ambiguity, thus in further investigations we will not consider this band gap.

The calculated magnonic band structures are presented in Fig. 4 with blue dashed and red solid lines for sample A and B, respectively. For MC with grooves the dispersion relation is symmetric and magnonic band gaps are opened at the Brillouin zone (BZ) border (first and third gap) and in the BZ center (the second gap). The frequencies of gaps obtained in calculations agree well with the gaps found in transmission measurements [Fig. 3(a)]. For sample B, the magnonic band structure is nonreciprocal, i.e., $f(k) \neq f(-k)$ [35,40]. Moreover, the first band has large slope (larger than for sample A), especially in the $+k$ direction which has significantly increased group velocity. These effects are related to conducting properties of the Au stripes, which cause suppressing of the dynamic magnetic field generated by oscillating magnetization in the areas occupied by metallic stripes for the wave which has amplitude localized at this surface [35]. Due to this nonreciprocity in the dispersion relation the magnonic band gap opens inside the BZ and it is an indirect band gap. Also for sample B we have found good agreement between calculations and measured data.

In the measured data shown in Fig. 3 there is visible difference between the width and depth of the first band gap in samples A and B. In order to estimate the depth of the gap from calculations we need to solve an inverse eigenproblem, i.e., to fix the frequency as a parameter and search for a complex wave number as an eigenvalue. In Fig. 5 the calculated imaginary part of the wave number (Im[k]) as a function of frequency around the first band gap is presented. In Figs. 5(a) and 5(b) the external magnetic field was set to 0.1 T; in Figs. 5(c) and 5(d) it was enlarged to the value 0.15 T. For sample A [Figs. 5(a) and 5(c)] the Im[k] has zero value outside of the gap since the Gilbert damping is neglected in the calculations. However, for sample B [Figs. 5(b) and 5(d)] the function Im[k](f) is nonzero outside of the gap; this is because the metal stripes induce attenuation of SWs. Outside of the gap regions in sample B the Im[k] increases with the frequency and this behavior is observed in the transmission spectra as a decrease of the signal at large frequencies (still in the transmission band of the reference sample) in sample B [Fig. 3(b)].

It is observed that the maximal value of Im[k] in the first band gap is significantly larger for sample B than A (0.113 and 0.062, respectively, for 0.1 T magnetic field). Because an inverse of Im[k] describes the decaying length of SWs, it correlates with the magnonic band gap depth in the transmission measurements. Indeed this finds confirmation in the experimental data, where the minimal transmission magnitude in the band gap is -18 dB at 4.81 GHz and -39 dB at 4.89 GHz in samples A and B, respectively. This significant suppression of the transmission of the SW signal in the first magnonic band gap in sample B is confirmed also in BLS measurements presented in Fig. 6, where two excitation frequencies were set to (a) 4.64 GHz and (b) 4.89 GHz. These frequencies were chosen to visualize the SW propagation at frequencies from the band and from the band gap, respectively. In both cases a decrease of the SW amplitude when increasing the distance from the transducer is found, however, in the band gap this decrease is more pronounced. Nevertheless, some signal is still observed at the end of MC for frequencies from the band gap. We suppose that this is due to the limited number of Au stripes used in the experiment and direct excitation of SWs from the transducer. The efficiency of the spin wave attenuation at forbidden frequency in these measurements might be affected also by the excitation of spin waves which do not propagate strictly in the direction perpendicular to the transducer's microstripe. It was shown that a bundle of spin

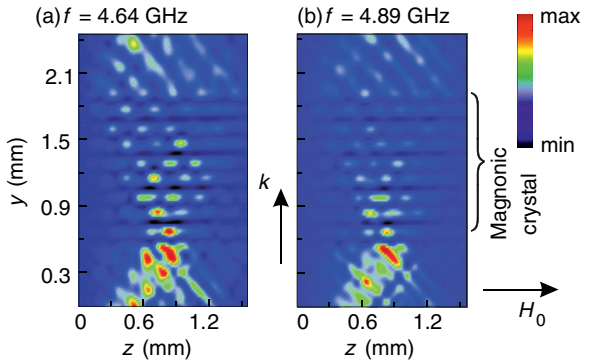

FIG. 6. (Color online) Maps of the SW intensity acquired with BLS from sample B at two frequencies (a) 4.64 GHz and (b) 4.89 GHz related to the transmission band and the band gap. The microstripe transducer aligned along the z axis used to excite SWs is located below the presented area.

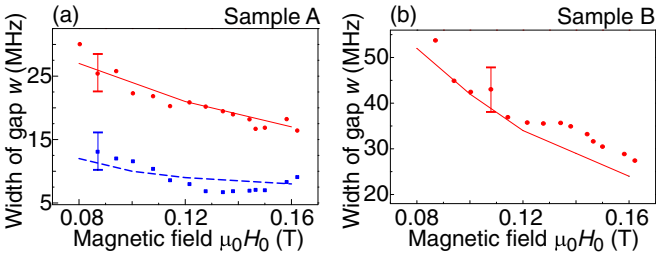

FIG. 7. (Color online) Width of the magnonic band gap as a function of the external magnetic field (a) in sample A and (b) in sample B. The experimental data are marked by full dots and squares, while the results of calculations are shown with solid and dashed lines for the first and second band gaps, respectively. The horizontal lines at some selected values of H_0 show errors of the measured magnonic band gap width.

waves with different values and directions of the wave vector are excited and create periodic interference patterns [41].

There is also another difference between function Im[k](f) for both samples. This is an asymmetry between the bottom and top part of the gap in sample B, while in sample A the function Im[k](f) is almost symmetric with respect to the magnonic band gap center. To have some measure of this asymmetry we have calculated the derivatives $\partial\mathrm{Im}[k]/\partial f$ at the points where Im[k] is half of its maximum value, i.e., at points a–d marked in Figs. 5(a) and 5(b). For sample A these values are 2.23×10^{-4} s/m and -2.28×10^{-4} s/m (points a and b, respectively) and for sample B 1.50×10^{-4} s/m and -1.97×10^{-4} s/m (respectively, points c and d).[1] We attribute this difference in Im[k] between MCs to the different group velocities of SWs around the gaps, i.e., the symmetric and asymmetric dispersion curves of the first (and second) band near the edge of the band gap for samples A and B, respectively (Fig. 4). We point out that this asymmetry in Im[k] might appear as an asymmetric slope in the transmission spectrum (Fig. 3) and it can be of importance for MC applications in magnetic field sensors and magnonic transistors [17,21]. This is because in the sensor proposed in Ref. [21] the slope of the band gap is decisive for the high sensitivity (the larger the slope, the larger the change of transmission of the SW on the small change of the magnetic field). In the operation of the magnonic transistors proposed in Ref. [17] the important is the proximity of the frequency of the carrier SWs to the magnonic band edge and also to the frequency of the injected magnons. Injected magnons steer the transmission of SWs, however, these magnons need to be localized in space (to avoid their escaping), thus their frequency shall be from the band gap of the MC.

Finally, we study magnonic band gap widths in dependence on the amplitude of the external magnetic field. The results are presented in Figs. 7(a) and 7(b) for samples A and B, respectively. In this figure there are points (full dots and squares) extracted from the transmission measurements and lines (red solid and blue dashed) obtained from FEM calculations (first and second band gaps, respectively). Overall, we have found good agreement between theory and measurements; the calculation results are always in the range of the experimental errors marked in the figures by solid vertical lines. The decrease of the band gap width with an increase of the magnetic field we attribute to the decrease of the band width (i.e., decrease of the group velocity) of the MSSW [42]. The steeper decrease of the band gap width is observed for the MC with metallic stripes. These dependencies also reflect the values of Im[k] shown in Fig. 5, where the Im[k] drops down by 23% in sample B, while for sample A the Im[k] remains almost the same with the increase of the magnetic field by 0.05 T.

These different dependencies for samples A and B are related to the larger sensitivity of the group velocity (v_g) of MSSW on changes of the magnetic field in metallized film than in unmetallized, but also to the nonreciprocal magnonic band structure and the presence of the indirect band gap in the case of sample B. The sensitivity of the group velocity around the gap might be estimated analytically. In Fig. 8 the analytical dispersion relation of MSSW in 10-μm thick YIG film with a metal overlayer is presented in the empty lattice model (ELM). The periodicity was taken the same as a periodicity of the samples. The crossing point between dispersions of the MSSW propagating in opposing directions, $+k$ (with maximum of the amplitude close to the metal) and $-k$ (with amplitude on the opposite surface, this dispersion is shifted in the figure by the reciprocal lattice vector $2\pi/a$) indicates the Bragg condition, i.e., the condition for opening the magnonic band gap. It means that the Bragg condition takes wave numbers from the first and second BZ for waves propagating into positive ($+k$) and negative ($-k$) directions of the wave vector, respectively [39,43]. The group velocities were calculated at crossing points at field values 0.1 T and 0.15 T for the YIG film with and without the metal overlayer. Based on these values, we have found that the ratio of the group velocities $[v_g(+k)/v_g(-k)]$ changed with the field and it is almost twice higher in structure with the metal layer than without metal.

Although the change of the dispersion slope around the Bragg condition is larger for the $+k$ wave, the magnitude of the wave vector $|+k|$ is smaller than $|-k|$ and the small change

[1]The small difference of the absolute values of the derivatives at points a and b for sample A is probably due to the asymmetry of the structure across the thickness (the grooves were etched only at one side).

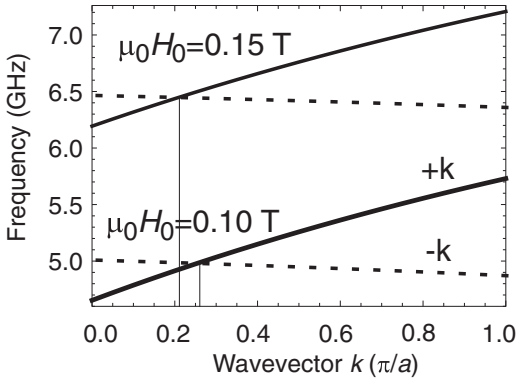

FIG. 8. Analytical estimation of the Bragg condition for the magnonic band gap opening in 10-μm thick metallized YIG film with periodicity $a = 150$ μm at two values of the external magnetic field: 0.1 T and 0.15 T. Dispersion relation of the propagating MSSW waves with maximum of the amplitude close to the metal (k^+) and on opposite side (k^-) of the film are marked with solid and dashed lines, respectively. The dispersion of the k^- wave is shifted by the reciprocal lattice vector $2\pi/a$ from its original position. The Bragg condition is fulfilled at the cross section of the k^+ and k^- lines.

of the group velocity of the $-k$ wave might also have an impact on change of the band gap position. In our case, the increase of the magnetic field from 0.1 T to 0.15 T results in a shift of the Bragg condition towards the BZ center from $k = 0.26$ to 0.21 in units π/a (see Fig. 8). However, in general, the position of the Bragg condition might shift towards the center or edge of the BZ with the increase of the field. The direction of the Bragg condition shift is determined by both the group velocity change and the wave number difference of MSSW propagating in opposite directions. We note also, that for both samples, the width of the second band gap is less sensitive to the magnetic field amplitude than the width of the first gap.

It is also sample B which has a wider band gap than sample A in the considered magnetic field values [see Figs. 7(a) and 7(b)]. It was already shown that covering the bi-component MC or ferromagnetic film with a lattice of grooves by a homogeneous metallic overlayer shall increase the band gap width of the MSSW due to increased group velocity of MSSW propagating along the metallized surface [43,44]. However, the influence of metal with finite conductivity depends on the wave number (and film thickness), and disappears for large k [35]. Thus, the band gap width will depend on the wave number at which the Bragg condition is fulfilled, i.e., will depend on the lattice constant. For sufficiently large k (small period) the influence of metal disappears and band gaps will not form [43]. In the homogeneous YIG film of 10-μm thickness the influence of the homogeneous Au overlayer on the dispersion relation of MSSW disappears for $k \approx 1.57 \times 10^6$ rad m^{-1}, i.e., for the MC with a period $a = 2$ μm at the BZ border the effect of metallization will be absent. The influence of metal will disappear also when the separation between metallic stripes and YIG will be introduced, however, this can be avoided by proper fabrication technique.

In sample A an influence of the corrugation shall preserve also for small a, thus it is expected that for the small lattice constant the band gap in sample A will be wider than for sample B. However, we note also that the band gap width depends also on the groove depth in sample A, thus there is an additional parameter to be taken into account. In the case of small surface perturbations (small ratio of the groove depth to the film thickness) the coupled mode theory shows that the width of the gap and the gap depth (maximal Im[k] in the gap) are proportional to the perturbation [15]. Nevertheless, the structure with larger grooves has not been found very promising for magnonic band gap applications so far, because of the suppressed transmission in the bands due to excitations of the standing spin waves [11,12,45]. This can change when the very thin YIG samples will be used for MCs; then the frequency of standing exchange SW modes will be moved to high frequencies. However, the fabrication of regular modulation of the film thickness in deep nanoscale remains a challenging task.

V. CONCLUSIONS

We have fabricated two planar 1D MCs in the form of a YIG film with a periodic array of etched grooves or metallic (Au) stripes atop. We have studied the properties of SWs propagating in the fabricated structures, and the magnonic band gaps in their SW spectra. The SW spectra have been investigated experimentally and theoretically. The obtained theoretical results are in good agreement with the measurement data. Fundamental differences have been found in the magnonic band structures of the two MCs, which also differ in the properties of their band gaps. We have shown that the MC with metallic stripes has a wider and deeper band gap compared to the MC with etched grooves. In both structures the width of the magnonic band gap decreases with increasing external magnetic field. However, in the MC with Au stripes the decrease in the band gap width is significantly steeper. We have performed a detailed study of the dispersion curves with a supplementary analysis of the imaginary part of the wave number to identify and explain the mechanisms behind the different dependencies found in the two structures. The indirect character of the band gap and the large group velocity of SWs in the MC with metallic stripes have been identified as the main underlying causes of the observed differences. Both result from the nonreciprocity introduced to the SW spectrum by the metallic stripes.

Considering that the fabrication of arrays of metallic stripes is much easier than the etching of grooves in a dielectric slab, and that the studied structure with Au stripes has a wider magnonic band gap compared to the structure with grooves, MCs with an array of metallic stripes atop might be a better solution for applications. However, the influence of the metal overlayer on the band gaps for magnetostatic waves is limited to relatively small wave numbers, which hinders the miniaturization prospects for these MCs. The other MC, based on a lattice of grooves, does not have such limitations, but the width and depth of its band gap are limited by the excitation of standing exchange SWs. The discussed properties will be of special importance for magnonic devices, such as magnetic field sensors [21] or fully magnonic transistors [17], the functionalities of which have already been demonstrated experimentally. The tailoring of the width and depth of the magnonic band gaps and the slope of their edges can be crucial for rendering magnonic devices competitive with the existing technologies.

ACKNOWLEDGMENTS

The research leading to these results has received funding from Polish National Science Centre Project No. DEC-2-12/07/E/ST3/00538, the European Union's Horizon 2020 research and innovation programme under Marie Skłodowska-Curie Grant No. 644348 (MagIC), SYMPHONY project operated within the Foundation for Polish Science Team Programme co-financed by the EU European Regional Development Fund, Grant No. OPIE 2007-2013, and Megagrant of the Government of the Russian Federation, Grant No. 2013-220-04-350.

[1] M. Krawczyk and H. Puszkarski, Acta Phys. Pol. A **93**, 805 (1998).
[2] S. A. Nikitov, P. Tailhades, and C. S. Tsai, J. Magn. Magn. Mater. **236**, 320 (2001).
[3] H. Puszkarski and M. Krawczyk, Solid State Phenomena **94**, 125 (2003).
[4] C. G. Sykes, J. D. Adam, and J. H. Collins, Appl. Phys. Lett. **29**, 388 (1976).
[5] M. Krawczyk and H. Puszkarski, Phys. Rev. B **77**, 054437 (2008).
[6] V. V. Kruglyak, S. O. Demokritov, and D. Grundler, J. Phys. D: Appl. Phys. **43**, 264001 (2010).
[7] S. O. Demokritov and A. N. Slavin, editors, *Magnonics from Fundamentals to Applications* (Springer, New York, 2013).
[8] M. Krawczyk and D. Grundler, J. Phys.: Cond. Matter **26**, 123202 (2014).
[9] J. Gouzerh, A. A. Stashkevich, N. G. Kovshikov, V. V. Matyushev, and J. M. Desvignes, J. Magn. Magn. Mater. **101**, 189 (1991).
[10] K. Chi, Y. Zhu, R. Mao, S. Nikitov, Y. Gulyaev, and C. Tsai, IEEE Trans. Magn. **47**, 3708 (2011).
[11] A. Chumak, A. Serga, S. Wolff, B. Hillebrands, and M. Kostylev, Appl. Phys. Lett. **94**, 172511 (2009).
[12] A. Chumak, A. Serga, S. Wolff, B. Hillebrands, and M. Kostylev, J. Appl. Phys. **105**, 083906 (2009).
[13] Y. Filimonov, E. Pavlov, S. Vysotstkii, and S. Nikitov, Appl. Phys. Lett. **101**, 242408 (2012).
[14] N. Kanazawa, T. Goto, and M. Inoue, J. Appl. Phys. **116**, 083903 (2014).
[15] S. R. Seshadri, J. Appl. Phys. **49**, 6079 (1978).
[16] K. W. Reed, J. M. Owens, and R. L. Carter, Circuits Systems Signal Process **4**, 157 (1985).
[17] A. V. Chumak, A. A. Serga, and B. Hillebrands, Nat. Commun. **5**, 4017 (2014).
[18] Y. Zhu, K. Chi, and C. Tsai, Appl. Phys. Lett. **105**, 022411 (2014).
[19] J. Owens, C. Smith, S. Lee, and J. Collins, IEEE Trans. Magn. **14**, 820 (1978).
[20] M. Dokukin, K. Togo, and M. Inoue, J. Magn. Soc. Jpn. **32**, 103 (2008).
[21] M. Inoue, A. Baryshev, H. Takagi, P. B. Lim, K. Hatafuku, J. Noda, and K. Togo, Appl. Phys. Lett. **98**, 132511 (2011).
[22] H. Takagi, J. Noda, T. Ueno, N. Kanazawa, Y. Nakamura, and M. Inoue, Electron. Comm. Jpn. **97**, 11 (2014).
[23] S.-K. Kim, J. Phys. D: Appl. Phys. **43**, 264004 (2010).
[24] J. W. Kłos, D. Kumar, J. Romero-Vivas, H. Fangohr, M. Franchin, M. Krawczyk, and A. Barman, Phys. Rev. B **86**, 184433 (2012).
[25] R. D. McMichael and B. B. Maranville, Phys. Rev. B **74**, 024424 (2006).
[26] J. W. Klos, D. Kumar, M. Krawczyk, and A. Barman, Sci. Rep. **3**, 2444 (2013).
[27] S. Pal, J. W. Klos, K. Das, O. Hellwig, P. Gruszecki, M. Krawczyk, and A. Barman, Appl. Phys. Lett. **105**, 162408 (2014).
[28] N. Singh, S. Goolaup, and A. Adeyeye, Nanotechnology **15**, 1539 (2004).
[29] A. Adeyeye, S. Jain, and Y. Ren, IEEE Trans. Magn. **47**, 1639 (2011).
[30] H. Chang, P. Li, W. Zhang, T. Liu, L. Hoffmann, A. Deng, and M. Wu, IEEE Magn. Lett. **5**, 6700104 (2014).
[31] H. Yu, O. Kelly, V. Cros, R. Bemard, P. Bortolotti, A. Anane, F. Brandl, R. Huber, I. Stasinopoulos, and D. Grundler, Sci. Rep. **4**, 6848 (2014).
[32] A. G. Gurevich and G. A. Melkov, *Magnetization Oscillations and Waves* (CRC-Press, Boca Raton, 1996).
[33] S. Demokritov, B. Hillebrands, and A. Slavin, Phys. Rep. **348**, 441 (2001).
[34] G. Raju, *Antennas and Wave Propagation* (Pearson Education, New York, 2006).
[35] M. Mruczkiewicz and M. Krawczyk, J. Appl. Phys. **115**, 113909 (2014).
[36] Z. K. Wang, V. L. Zhang, H. S. Lim, S. C. Ng, M. H. Kuok, S. Jain, and A. O. Adeyeye, Appl. Phys. Lett. **94**, 083112 (2009).
[37] K. H. Chi, Y. Zhu, R. W. Mao, J. P. Dolas, and C. S. Tsai, J. Appl. Phys. **109**, 07D320 (2011).
[38] M. Mruczkiewicz, M. Krawczyk, V. K. Sakharov, Y. V. Khivintsev, Y. A. Filimonov, and S. A. Nikitov, J. Appl. Phys. **113**, 093908 (2013).
[39] M. Mruczkiewicz, M. Krawczyk, G. Gubbiotti, S. Tacchi, Y. A. Filimonov, D. V. Kalyabin, I. V. Lisenkov, and S. A. Nikitov, New J. Phys. **15**, 113023 (2013).
[40] I. Lisenkov, D. Kalyabin, S. Osokin, J. Klos, M. Krawczyk, and S. Nikitov, J. Magn. Magn. Mater. **378**, 313 (2015).
[41] V. E. Demidov, P. Rekers, B. Mahrov, and S. O. Demokritov, Appl. Phys. Lett. **89**, 212501 (2006).
[42] D. Stancil and A. Prabhakar, *Spin Waves: Theory and Applications* (Springer, New York, 2009).
[43] M. Mruczkiewicz, E. S. Pavlov, S. L. Vysotsky, M. Krawczyk, Y. A. Filimonov, and S. A. Nikitov, Phys. Rev. B **90**, 174416 (2014).
[44] M. L. Sokolovskyy, J. W. Kłos, S. Mamica, and M. Krawczyk, J. Appl. Phys. **111**, 07C515 (2012).
[45] R. L. Carter, C. V. Smith, and J. M. Owens, IEEE Trans. Magn. **16**, 1159 (1980).